JPn Neuroscience
The Journal of Physiology

Looping circuit: a novel mechanism for prolonged spontaneous $[Ca^{2+}]_i$ increases in developing embryonic mouse brainstem

Hirofumi Watari[1], Amanda J. Tose[2] and Martha M. Bosma[1,2]

[1]*Graduate Program in Neurobiology & Behaviour and* [2]*Department of Biology, University of Washington, Seattle, WA, USA*

Key points

- Calcium concentration is kept at extremely low levels inside brain cells; each episode of calcium entry is cleared within seconds.
- Changes in calcium entry are mediated by spontaneous activity in embryonic mouse brainstem from embryonic day 11.5 to 13.5.
- Transiently, at embryonic day 12.5, spontaneous events occur frequently such that calcium concentration stays above baseline levels for minutes.
- This unusual phenomenon, which we termed 'bash bursts', is caused by an event that propagates by looping along a defined path; the path gets modified a day later, ending it.
- The results help us to understand how prolonged increases in calcium concentration can occur in development and how the increases may influence the development of serotonin and dopamine circuits that are related to neurological diseases later in life, such as depression and Parkinson's disease.

Abstract Most cells maintain $[Ca^{2+}]_i$ at extremely low levels; calcium entry usually occurs briefly, and within seconds it is cleared. However, at embryonic day 12.5 in the mouse brainstem, trains of spontaneous events occur with $[Ca^{2+}]_i$ staying close to peak value, well above baseline, for minutes; we termed this 'bash bursts'. Here, we investigate the mechanism of this unusual activity using calcium imaging and electrophysiology. Bash bursts are triggered by an event originating at the mid-line of the rostral hindbrain and are usually the result of that event propagating repeatedly along a defined circular path. The looping circuit can either encompass both the midbrain and hindbrain or remain in the hindbrain only, and the type of loop determines the duration of a single lap time, 5 or 3 s, respectively. Bash bursts are supported by high membrane excitability of mid-line cells and are regulated by persistent inward 'window current' at rest, contributing to spontaneous activity. This looping circuit is an effective means for increasing $[Ca^{2+}]_i$ at brief, regular intervals. Bash bursts disappear by embryonic day 13.5 via alteration of the looping circuit, curtailing the short epoch of bash bursts. The resulting sustained $[Ca^{2+}]_i$ may influence development of raphe serotonergic and ventral tegmental dopaminergic neurons by modulating gene expression.

H. Watari and A. J. Tose contributed equally to this work.

DOI: 10.1113/jphysiol.2013.265892

(Received 24 September 2013; accepted after revision 17 December 2013; first published online 23 December 2013)
Corresponding author M. M. Bosma: Department of Biology, Box 351800, University of Washington, Seattle, WA 98195, USA. Email: martibee@uw.edu

Abbreviations ACSF, artificial cerebrospinal fluid; Bash-B, bash bursts; E, embryonic day; InZ, initiation zone; r, rhombomere; V_{rest}, resting membrane potential.

Introduction

In most cells, $[Ca^{2+}]_i$ levels are tightly regulated and changes are brief, allowing $[Ca^{2+}]_i$ fluxes to have significant biological actions, such as synaptic release and modulation of gene expression. In many regions of the developing nervous system, including the brainstem (Bosma, 2010), calcium is introduced into the cytoplasm by spontaneous activity, which plays an important role in developmental processes such as proliferation, differentiation, migration, axonal pathfinding, synaptogenesis and neurotransmitter specification (Moody & Bosma, 2005; Spitzer, 2012). In this report, we present an unusual phenomenon where $[Ca^{2+}]_i$ is raised above baseline levels in a sustained, pulsatile waveform for prolonged periods of time.

Spontaneous activity occurs during embryonic days (E) 10.5–13.5 in the mouse brainstem (Hunt *et al.* 2006*b*; Rockhill *et al.* 2009). Most events originate in the initiation zone (InZ; Moruzzi *et al.* 2009), located at the hindbrain mid-line in former rhombomere (r) 2; events then propagate rostrocaudally along the mid-line of the hindbrain (Hunt *et al.* 2006*b*). This spontaneous activity is a distinct phenomenon from depolarization waves that originate in the spinal cord (Momose-Sato *et al.* 2012), because the location of the InZ is unaffected by removal of the spinal cord. At E12.5, some events propagate rostrally across the midbrain–hindbrain border (isthmus) and into the midbrain tegmentum. This propagation may occur on tracts of serotonergic axons that extend rostrally through that region (Rockhill *et al.* 2009). From E13.5 to 14.5, the extent of propagation retracts, and events finally disappear due to a progressive increase in the resting potassium conductance and hyperpolarization of the resting membrane potential (V_{rest}; Watari *et al.* 2013).

Hindbrain spontaneous activity is driven by membrane depolarization that involves Ni^{2+} and mibefradil-sensitive Ca_V3 channels mediating T-type Ca^{2+} current (Moruzzi *et al.* 2009). These depolarizations resemble conventional action potentials in overshooting 0 mV when beginning from a relatively hyperpolarized V_{rest}. Unlike conventional action potentials, however, depolarizations that underlie spontaneous activity consist of a brief spike followed by a long plateau, lasting for up to 1 s before repolarizing to rest (Moruzzi *et al.* 2009). Resting membrane potential can range widely, depending on the developmental stage and location in the hindbrain; cells positioned closer to the InZ show more depolarized potentials during the window of spontaneous electrical activity (E11.5–13.5; Watari *et al.* 2013). Each depolarization leads to, and is outlasted by, an increase in $[Ca^{2+}]_i$, causing each calcium event to last approximately 6 s (Watari *et al.* 2013).

Here, we report a novel propagation pattern that underlies a previously uncharacterized phenomenon called 'bash bursts' (Bash-B), in which $[Ca^{2+}]_i$ rises above baseline for, in some cases, longer than 10 min. We show that a looping circuit is an effective mechanism by which participating cells can experience calcium influx at frequent and regular intervals. Bash bursts emerge at E12.5 and disappear within 24 h due to alteration of the looping circuit, making Bash-B stage specific. These bouts of sustained increase in $[Ca^{2+}]_i$ may modulate gene expression necessary for the development of the rostral brainstem, including the raphe serotonergic and tegmental dopaminergic neurons that develop along the paths of spontaneous activity.

Methods

Ethical approval

All animal care procedures were approved by University of Washington Animal Care Committee (IACUC).

Animals and dissections

Timed-pregnant Swiss/Webster mice were killed by inhalation of CO_2 followed by cervical dislocation. Embryos from E10.5 to 15.5 were maintained for up to 10 h in artificial cerebrospinal fluid (ACSF) containing (mM): 119 NaCl, 2.5 KCl, 1.3 $MgCl_2$, 2.5 $CaCl_2$, 1 NaH_2PO_4, 26 $NaHCO_3$ and 30 glucose, oxygenated with carbogen (5% CO_2 and 95% O_2). When the brainstem (midbrain, hindbrain and cerebellar flap) was dissected out, the hindbrain naturally lay flat in an open-book configuration; the midbrain was cut along its dorsal mid-line so that it lay flat along with the hindbrain. Some calcium imaging recordings were done on brainstem preparations with the spinal cord attached ($n = 5$), demonstrating that the process of initiation of spontaneous activity was unchanged in the presence of the spinal cord. Some patch-clamp recordings that did not require the midbrain were performed on isolated hindbrains. The

mesenchyme was removed in all preparations with one exception; a small patch of mesenchyme was left attached on some E11.5 brainstem preparations around the midbrain tegmental area to avoid pulling on cranial nerve III and damaging the area. The dissected tissue was bath perfused in oxygenated ACSF at the rate of 1 ± 0.3 ml min^{-1} for up to 2 h, after which the experiment was terminated. Osmolarity of the oxygenated solution was 316 ± 1 mosmol l^{-1}. All experiments were done at approximately 23°C.

Calcium imaging

The brainstem was dissected out and incubated in oxygenated ACSF with 1.9 μM Quest fluo-8 AM (AAT Bioquest, Inc., Sunnyvale, CA, USA) and 0.075% Pluronic F-127 (Sigma-Aldrich, St Louis, MO, USA) for 15 min at 23°C. Changes in fluorescence were measured in up to 83 regions of interest using a ×10 objective for r2 InZ experiments and a ×4 objective for midbrain–hindbrain experiments. $\Delta F/F$ values were recorded using Metafluor (Molecular Devices, LLC, Sunnyvale, CA, USA) and CoolSNAP HQ^2 (Photometrics, Tucson, AZ, USA) with shutter speeds of 1 or 2.43 Hz. Data were visualized and analysed using ImageJ (National Institutes of Health, Bethesda, MD, USA), Excel (Microsoft Corp., Redmond, WA, USA) and Igor Pro (Wavemetrics, Inc., Lake Oswego, OR) with custom functions developed by H.W. The baseline of the $\Delta F/F$ traces was corrected for drift caused by photobleaching in the same way as it was done previously (Watari *et al.* 2013). Drift was detected semi-automatically using a custom-written Igor Pro function, by sampling $\Delta F/F$ values at an interval of every 20 data points. The sampling was then manually corrected so that events were not inadvertently affected, and the resulting traces were stacked. For line intensity scan analysis, individual pixels from image sequences containing two to five propagating events were compiled into a single image based on the value of the highest intensity recorded at each pixel. The resulting image was smoothed by the Gaussian bicubic method. The line scan was performed across the mid-line axis every 200 μm from the isthmus to r2 on the hindbrain and across the midbrain tegmentum 100 μm rostral to the isthmus; each line scan was repeated over the rostrocaudal area covering 20 μm × 400 μm, and the averaged result was then plotted. The traces were normalized by dividing $\Delta F/F$ values by the peak amplitudes of each line scan. Statistics for the correlation analysis was done using Pearson's *r*.

Electrophysiology

Internal solution contained the following (mM): 100 potassium gluconate, 15 KCl, 1 EGTA, 5 $MgCl_2$, 40 Hepes, 3 Na-ATP and 0.3 Na-GTP; pH was titrated to 7.25 by addition of NaOH, and osmolarity was adjusted to 328 ± 2 mosmol l^{-1} by addition of sucrose. Some patch-clamp experiments were done on isolated hindbrain preparations with the midbrains removed, but the results did not differ from recordings done on midbrain–hindbrain preparations; therefore, all data were pooled. For voltage-step experiments, *P*/–4 leak subtraction was applied online to expose a component of current that is voltage dependent. Data were acquired using an Axopatch 200B amplifier and pCLAMP software (Molecular Devices) in the same conditions as described previously (Watari *et al.* 2013). Data were analysed using Igor Pro with custom functions provided by H.W. and NeuroMatic (Jason Rothman). All statistics, unless indicated otherwise, were one-way ANOVA. If the result of group comparison was significant, multiple comparison Tukey's (HSD) test was performed *post hoc*. Significance is indicated as $^*P < 0.05$, $^{**}P < 0.01$ and $^{***}P < 0.001$.

Results

Sustained $[Ca^{2+}]_i$ in mid-line cells of rostral brainstem at E12.5

Spontaneous activity originates at the initiation zone, which is predominantly located at the mid-line of former rhombomere 2 (Fig. 1*A*, grey box; Hunt *et al.* 2006*a*; Moruzzi *et al.* 2009), which lies along the mid-line group of raphe serotonergic neurons (situated from the isthmus to r4). At E12.5, events originating from the InZ can be followed by a bout of high-frequency calcium events arriving from the more rostral mid-line of the hindbrain. An example of this is shown in Fig. 1*B*, where a train of four calcium waves propagate caudally after an InZ-initiated event (*; event not shown), with wavefronts spaced approximately 300 μm apart from each other (calcium events labelled a, b, c and d in panels 1.2–14.8 s of Fig. 1*B*). These calcium events summate (Fig. 1*C*, middle panel); that is, the level of $[Ca^{2+}]_i$ does not return to baseline before the next $[Ca^{2+}]_i$ event arrives. This type of $[Ca^{2+}]_i$ transient summation occurs infrequently at E11.5 ($n = 3$ of 18 experiments); most events occur from a defined baseline (Fig. 1*C*, left panel). At E13.5, events do not summate in normal conditions ($n = 8$; Fig. 1*C*, right panel). Here, we characterize the high-frequency $[Ca^{2+}]_i$ events that prevail at E12.5.

Within these trains, each event peak is followed by another peak before the $[Ca^{2+}]_i$ returns to baseline, with the consequence that the mid-line cells experience above-baseline $[Ca^{2+}]_i$ for a mean of 79.5 ± 8.2 s ($n = 206$, 62 preparations); the longest episode lasted 12 min 19 s (Fig. 1*D*). These instances of high-frequency $[Ca^{2+}]_i$ events are called 'bash bursts' (Bash-B). Bash bursts occur in 78.9% of E12.5 litters (30 of 38 litters, recording from

at least three brainstems per litter). Of those litters, 58% of brainstem preparations ($n = 61$ of 105 total) showed an average of 3.44 ± 0.29 separate instances of Bash-B, while the remaining preparations did not show Bash-B during the 30 min recording period. Each tissue that showed Bash-B spent 15% (4 min 34 s) of the 30 min recording period undergoing Bash-B, leading to sustained $[Ca^{2+}]_i$.

Events that resulted in Bash-B were arriving from a more rostral region than former r2 (Fig. 1*B*). To investigate where these events originate and how their frequency is set, we performed calcium imaging using a low-magnification objective (Fig. 2) to view the InZ as well as rostral regions up to and including the midbrain tegmentum, a region relevant to proliferation and differentiation of dopaminergic neurons.

A typical episode of Bash-B begins with an event that initiates at the InZ (* at 0 s in Fig. 2). The InZ is located exclusively in the hindbrain ($n = 25$), as reported previously (Rockhill *et al.* 2009), although some initiations occurred more rostrally along the mid-line of the hindbrain between the isthmus and r2. An example of Bash-B is characterized by the following sequence. An event originates at the InZ and propagates rostrally along the mid-line (Fig. 2, 1.2–4.9 s) until it reaches the midbrain–hindbrain boundary, or isthmus (Fig. 2, dashed box; also see Fig. 3 at 4.9 s), and crosses it. After the event crosses the isthmus (Fig. 3, 5.7 s), it propagates first on the right side of the midbrain (Fig. 3, 6.2–6.6 s). The event then crosses the mid-line to reach the left side of the midbrain (Fig. 3, 7.0–7.8 s) and exits the midbrain by recrossing the isthmus and propagating back into the hindbrain (Fig. 3, 8.2 s). The event propagates caudally on the left side of the hindbrain mid-line (Fig. 3, 8.6–9.0 s), crosses over to the right side of the mid-line (Fig. 3, 9.4 s), and then bifurcates so that the event propagates both rostrally and caudally (Figs 2 and 3, 9.8 s). The caudally-directed component propagates along the mid-line tracks, passes through the InZ, and dissipates (Fig. 2, 11.1–16.0 s; bottom half of the panels). The other component propagates rostrally, reenters the midbrain, and the looping process repeats

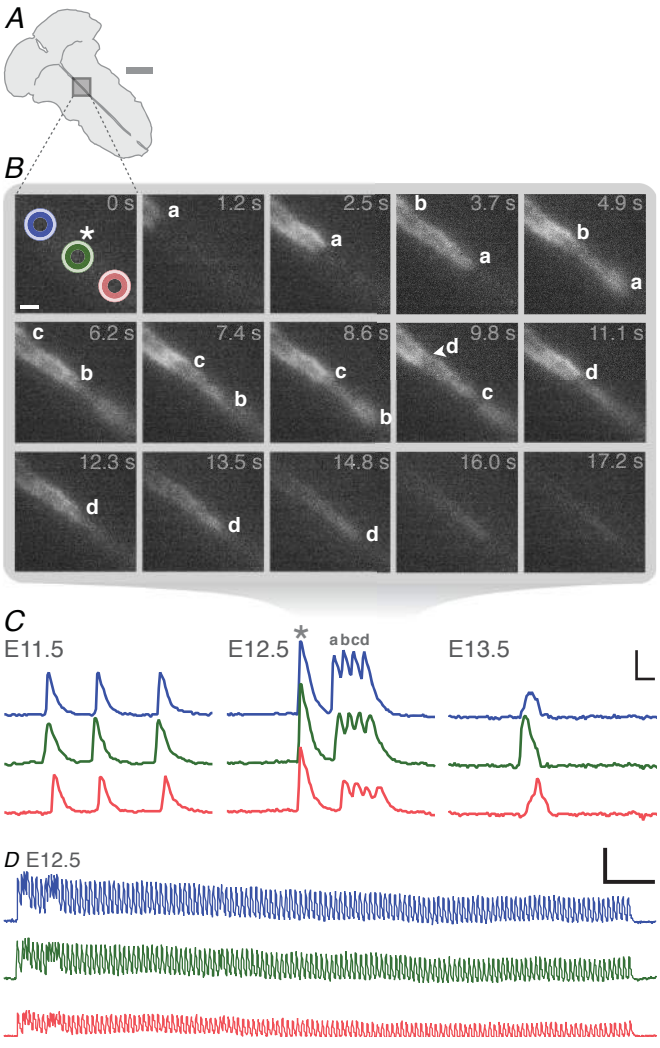

Figure 1. A sustained increase in $[Ca^{2+}]_i$ in the mid-line of the hindbrain at embryonic day (E) 12.5
A, position of $[Ca^{2+}]_i$ imaging on rhombomere (r) 2 of the hindbrain mid-line. Scale bar represents 1 mm. *B*, image sequence of high-frequency spontaneous activity recorded at E12.5. The position of event initiation (not shown in this sequence) is indicated as * at 0 s. The change in fluorescence is measured in three regions of interest, placed along the mid-line as shown at 0 s. The colours of the three regions of interest correspond to the colours of the $\Delta F/F$ *vs.* time traces shown in *C* and *D*. Recurrent calcium waves, indicated as a–d, propagate caudally along the mid-line of hindbrain (from 1.2 to 17.2 s); each wavefront appears from a more rostral part of the hindbrain (off screen in upper left corner of the image). Scale bar represents 100 μm. *C*, representative patterns of $[Ca^{2+}]_i$ events plotted as $\Delta F/F$ *vs.* time from E11.5 to 13.5, demonstrating different wave patterns at each of the three stages. At E11.5 (left panel), most $[Ca^{2+}]_i$ waves are recorded as single, discrete events. At E12.5 (middle panel), an event at the initiation zone (InZ; labelled *) is followed by multiple calcium waves that occur in rapid succession (labelled a–d); the resultant $[Ca^{2+}]_i$ events summate such that each peak in $[Ca^{2+}]_i$ occurs before $[Ca^{2+}]_i$ from the previous event returns to baseline. This episode of sustained $[Ca^{2+}]_i$ is referred to as 'bash bursts' (Bash-B). At E13.5 (right panel), events become less frequent and, as also observed at E11.5, do not summate. Each stage is represented by recordings from different brainstem preparations sampled at 2.43 Hz. Scale bar represents 3 $\Delta F/F$ and 5 s. *D*, one of the longest recorded durations of Bash-B is longer than 12 min, encompassing 129 calcium wave propagations. Scale bar represents 3 $\Delta F/F$ and 1 min.

itself (9.8 s and later in Figs 2 and 3). Several loops from this episode are shown at higher temporal resolution in Figs. 2, 3 and Movie 1, demonstrating the repetitive circular pattern of propagation at or near the isthmus. The event took approximately 5 s to loop around once. The $[Ca^{2+}]_i$ peaks every 5 s in the mid-line and tegmental cells, which is less than the amount of time it takes for $[Ca^{2+}]_i$ to return to baseline, resulting in Bash-B. This 5 s propagation pattern is referred to as the midbrain–hindbrain loop (Fig. 4*A*) because it involves a circuit that encompasses both the midbrain and the hindbrain, with the isthmus border acting as a 'pivot' at the mid-line, around which the event propagates.

In order to categorize the propagation patterns of the calcium wave that mediates Bash-B, we analysed the first recorded episode in each of 58 different brainstem preparations. While 37 of 58 episodes of Bash-B were due to loops involving tracks in both the midbrain and the hindbrain (63.8%; Fig. 4*A*), 19 of 58 episodes were due to loops that occurred exclusively in the hindbrain (hindbrain-only loops; 32.8%; Fig. 4*B*). Location was not the sole difference between these two types of loops; another critical difference was the lap time. While the mean lap time was 5.0 ± 0.3 s ($n = 7$) for the midbrain–hindbrain loops, the lap time was significantly faster for the hindbrain-only loop (3.0 ± 0.2 s,

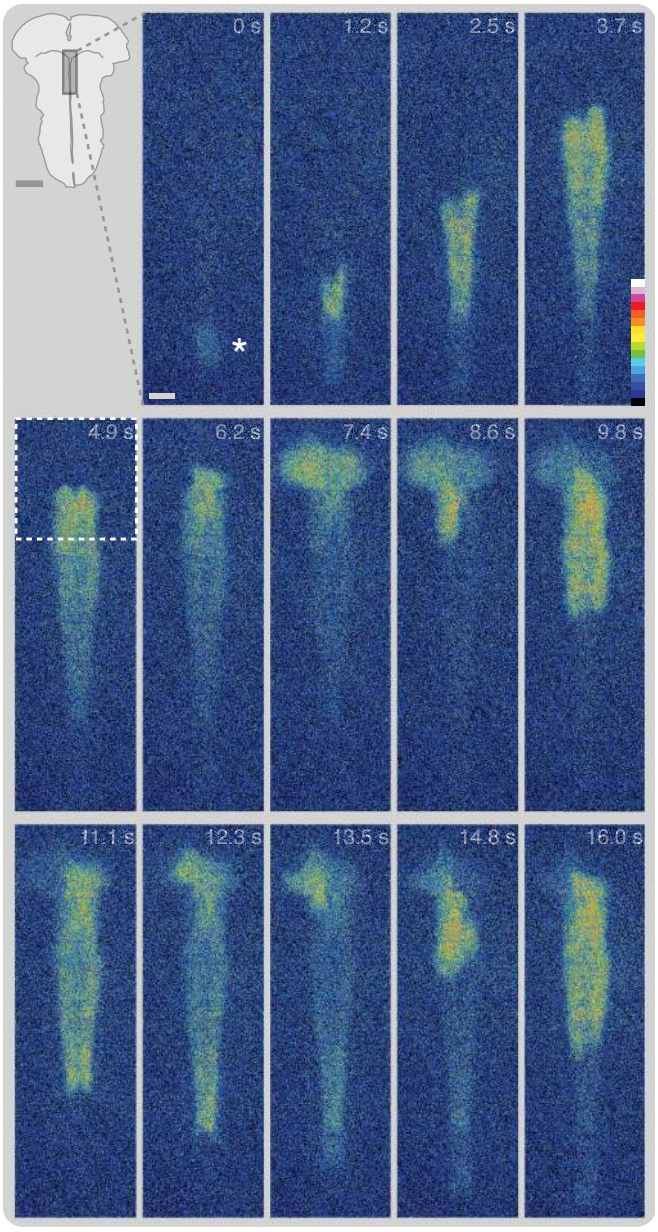

Figure 2. Bash bursts are the result of a looping calcium event at E12.5
Calcium imaging along the mid-line of the rostral brainstem using a low-magnification (×4) objective so that the InZ (* at 0 s) at r2 hindbrain and the midbrain tegmentum are included; camera position is indicated at the upper left corner (scale bar represents 1 mm). Panels of image sequences are shown starting at 0 s, when the $[Ca^{2+}]_i$ event initiates at the InZ (*). The event then propagates rostrocaudally (1.2 s), with the caudal portion disappearing from the bottom of the image (2.5 s). The event propagates rostrally (from 1.2 to 3.7 s) until its wavefront reaches the midbrain–hindbrain border, or isthmus (4.9 s). A sequence of higher temporal resolution image in the squared area (dotted line at 4.9 s) is captured in Fig. 3 to show the details of calcium wave propagation. The event enters the midbrain tegmentum (6.2 s), propagates contralaterally (7.4 s), crosses the isthmus caudally and propagates back into the hindbrain (8.6 s), and then splits so that one portion of the event propagates caudally (from 9.8 to 16.0 s), while the other portion propagates rostrally. The rostral portion then re-enters the midbrain (9.8 s), again propagates contralaterally across the midbrain (from 11.1 to 13.5 s), crosses the isthmus (14.8 s), and the whole cycle repeats itself (16.0 s). The images are pseudocoloured to show relative intensity of $[Ca^{2+}]_i$ (white, high intensity; black, low intensity). Scale bar represents 100 μm.

$n = 7$; $P < 0.001$). The consequence of a faster lap time is that it reduces the interval during which the cell can extrude cytoplasmic calcium before the next event arrives; therefore, the participating cells experience a higher average $[Ca^{2+}]_i$, closer to its peak $\Delta F/F$ value; this is in contrast to Bash-B with larger deflections in $[Ca^{2+}]_i$ caused by the midbrain–hindbrain loops. These distinct lap times are useful markers to predict the type of looping circuit during patch-clamp experiments where spatial information of the event propagation is absent.

Two of 58 episodes of Bash-B did not involve a looping circuit, but instead resulted from rapid repetitive firing at the InZ (3.4%; Fig. 4*C*, left half). A total of 15 episodes (25.9%) showed a switching of the looping mode: one of two rapid firing of the InZ switched to midbrain–hindbrain loops (Fig. 4*C*); four of 19 hindbrain-only loops switched to midbrain–hindbrain loops; and 10 of 37 midbrain–hindbrain loops switched to hindbrain-only loops (Fig. 4*D*), yielding $[Ca^{2+}]_i$ peaks at different intervals. The directionality of the loop could either be clockwise or anticlockwise, and a given preparation was capable of looping in either direction (Fig. 4*D*). However, the directionality was not entirely random for certain types of loops, which will be described in detail below.

Directionality is predictable for hindbrain-only loops

The brainstem inherently allows the event to loop either clockwise or anticlockwise, but after the first lap the event tends to continue to loop in the same direction. The directionality was predictable for the shorter (3 s) hindbrain-only loops, but not for the longer (5 s) midbrain–hindbrain loops. For the 3 s loops, the directionality was well correlated with the

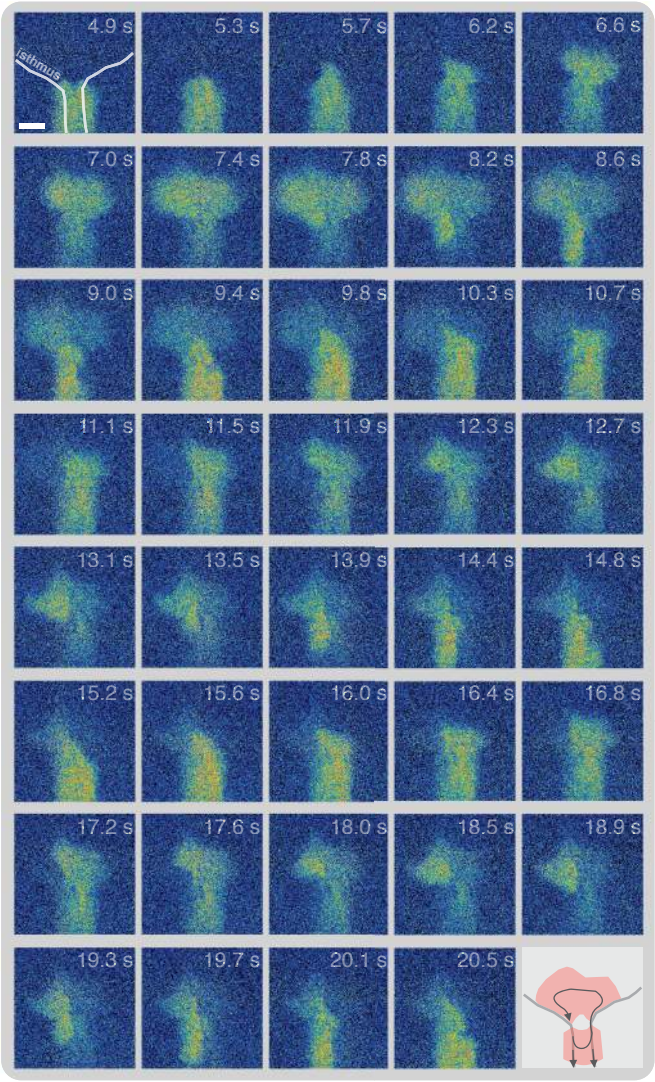

Figure 3. Midbrain–hindbrain loops underlie Bash-B and have a characteristic 5 s lap time
A looping circuit is shown that involves paths in the midbrain tegmentum and rostral hindbrain, imaged at high temporal resolution. The outline of the midbrain–hindbrain border (isthmus) and the two mid-line tracks in the hindbrain (vertical lines) are shown in the image in the upper left corner. The image sequence is taken directly from the squared area in Fig. 2 at 4.9 s. The calcium event propagates rostrally and crosses the isthmus at 5.3 s. The wavefront enters the midbrain tegmentum (5.7 s) and propagates on the right side of the midbrain tegmentum (6.2 s). It then propagates contralaterally to the left side of the midbrain (from 6.6 to 7.8 s), crosses the isthmus (8.2 s), and propagates caudally on the left mid-line track in the hindbrain (from 8.2 to 8.6 s). The event propagates contralaterally to the right mid-line track in the hindbrain (from 9.0 to 9.4 s) and bifurcates so that events propagate rostrocaudally along that right track. The rostral portion of the event crosses the isthmus, and the cycle repeats itself twice more anticlockwise (from 9.8 to 15.2 s and from 15.6 to 20.5 s). Note that each lap takes approximately 5 s. Bottom right is an illustration of the looping track and the direction of event propagation (arrows). Scale bar represents 100 μm.

side of the mid-line at which the event initiated ($r = 0.76$). When events initiated on the left side of the mid-line, they consistently looped clockwise ($n = 4$ of 4; Fig. 4*B*), whereas events that initiated on the right side turned anticlockwise ($n = 4$ of 5). Thus, for hindbrain-only loops, 88.9% ($n = 8$ of 9) of the directionality was set by the location on the mid-line at which the event initiated. In contrast, the directionality was less predictable for the 5 s midbrain–hindbrain loops ($r = -0.31$), with a lower probability of 36.4% ($n = 4$ of 11). An unknown process in the midbrain, perhaps related to refractory properties, seems to allow the event to turn in either direction and even to reverse direction.

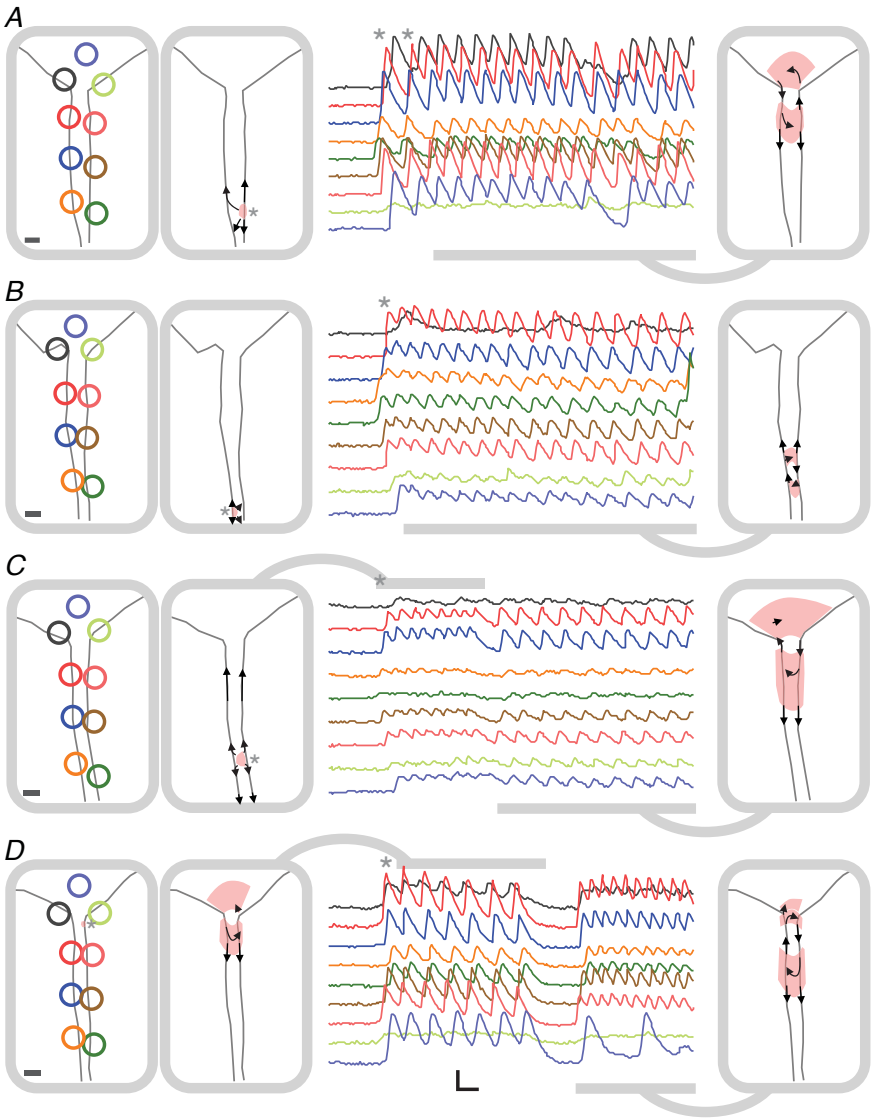

Figure 4. Variations of loops that underlie Bash-B
Four examples of Bash-B at E12.5. Every instance of Bash-B follows an initiating trigger (*) in the hindbrain and, with some exceptions, is comprised of one or more loop patterns. *A*, midbrain–hindbrain loops. *B*, hindbrain-only loops. *C*, a non-looping, rapid firing of InZ followed by midbrain–hindbrain loops. *D*, anticlockwise midbrain–hindbrain loops followed by clockwise hindbrain-only loops. During the latter loops, the event enters the midbrain tegmentum only sporadically (light blue trace). In *A–D*, three regions of interest in the left panels correspond to the colour-matched $\Delta F/F$ traces. Scale bar represents 100 μm. All traces are representative $\Delta F/F$ traces showing Bash-B. Scale bar represents 2 $\Delta F/F$ and 5 s. Panels to the sides of the traces illustrate the patterns of event propagation. The lengths of the arrows in the diagrams show the relative speed of propagation, where a short length indicates slower propagation. Illustrations depicting the looping tracks, locations of the InZ and directionality were created after video analysis, as in Fig. 3.

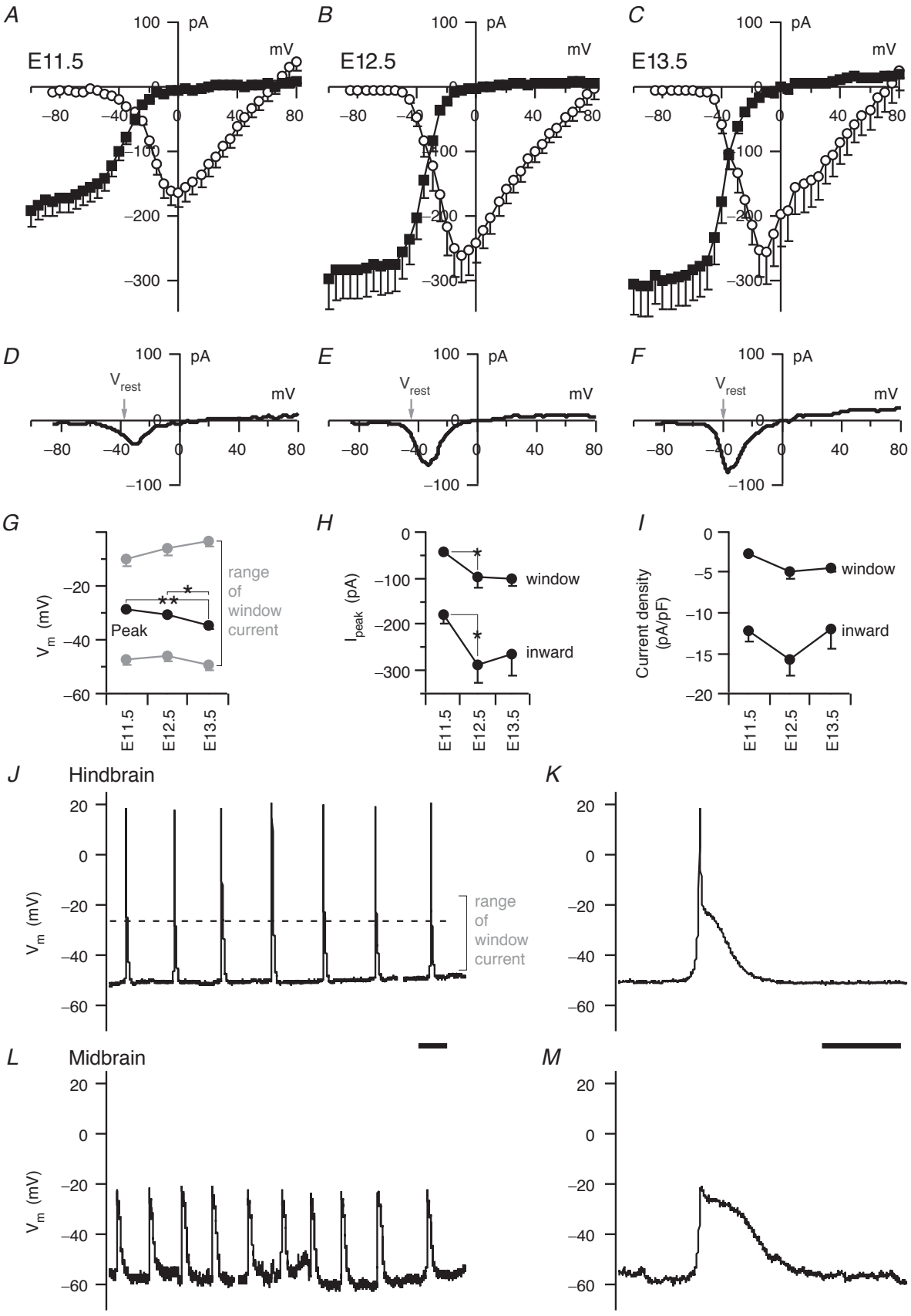

Membrane properties of InZ cells are primed to allow spontaneous events

The mid-line cells, including the cells at the InZ, have lower resting conductance and more depolarized V_{rest} compared with lateral cells. This makes them more excitable and supportive of spontaneous firing (Watari *et al.* 2013). Additionally, the mid-line cells display a relatively large voltage-gated inward current, which supports depolarization (Moruzzi *et al.* 2009); these combined features allow mid-line cells to experience more waves of $[Ca^{2+}]_i$ than lateral cells. However, Bash-B are a phenomenon that is most prevalent at E12.5, and a possible change in the membrane excitability may underlie its ability to sustain activity at the frequencies of the loops. We therefore performed voltage-clamp experiments on InZ cells from E11.5 to E13.5. In order to plot the activation curve for the inward current, the voltage was stepped from –80 to +80 mV in 5 mV increments; peak current amplitude (occurring within the first 34 ms) was measured and plotted against voltage (Fig. 5*A*–*C*, open circles).

At early stages, the predominant inward current is T-type calcium (Moruzzi *et al.* 2009), but starting at E12.5, the inward current appears to be a combination of Ni^{2+}-sensitive calcium current and TTX-sensitive sodium current ($n = 3$, data not shown). The voltage-gated ion channel that mediates the inward current inactivates rapidly with a mean time constant of 4.7 ± 1.0 ms ($n = 15$; the voltage was stepped from –80 to –10 mV). We measured the residual inward current after a prepulse and plotted the steady-state inactivation at each stage. The resulting inactivation curve (filled squares) is superimposed on the activation curve (Fig. 5*A*–*C*). This exposes the 'window current' (Fig. 5*D*–*F*), a persistent inward current that is known to occur for certain types of calcium currents, including the T-type (Capiod, 2011). The window current occurs in the range of voltages from −6.3 ± 2.9 to −46.2 ± 2.2 mV at E12.5 ($n = 16$), within which there is a net inward current (peaking at −30.9 ± 1.0 mV; Fig. 5*G*). At E12.5, the peak inward current increases significantly (E11.5, −178.4 ± 20.9 pA, $n = 18$ *vs.* E12.5, −289.3 ± 39.9 pA, $n = 16$; $P < 0.05$), as does the peak window current (E11.5, −40.9 ± 4.7 pA, $n = 18$ *vs.* E12.5, −97.7 ± 22.1 pA, $n = 16$; $P < 0.05$; Fig. 5*H*). In addition, the peak inward current density reaches its highest value at E12.5 (Fig. 5*I*), indicating that a relatively high density of voltage-gated ion channel types mediating inward current are expressed at this stage. As shown by the arrows (Fig. 5*D*–*F*), at every stage, the mean V_{rest} (Watari *et al.* 2013) lies within the voltage range of window current, suggesting that calcium may leak into the cytoplasm even at rest, contributing to spontaneous activity and continuous calcium influx. Therefore, window current may play a role in initiating spontaneous activity and setting V_{rest} itself by counterbalancing leak outward current. The increase in peak inward current and window current, coupled with relatively lower resting conductance (Watari *et al.* 2013), makes the InZ cells at E12.5 one of the most excitable cell types in this system across stages, and thereby makes them able to support event initiation necessary for Bash-B.

The existence of window current suggests that InZ cells can undergo sustained influx of calcium, resulting in Bash-B, by persistent membrane depolarization near the voltage of peak window current (−30.9 ± 1.0 mV at E12.5, $n = 16$; Fig. 5*G*). We investigated this possibility by performing current clamp of an r1 hindbrain cell, which is typically included in the pathway of Bash-B propagation. The recording shows an example of membrane potential during a midbrain–hindbrain loop (Fig. 5*J*). Each depolarizing event shows a characteristic waveform, with a fast-rising peak that overshoots 0 mV followed by a slower plateau (Fig. 5*K*; Moruzzi *et al.* 2009). Instead of maintaining the voltage around the peak of window current (dashed line in Fig. 5*J*; −26.4 mV for this cell), each depolarizing event repolarizes fully back to V_{rest} (−49.6 ± 0.4 mV for this cell) before the next depolarization. The trace is unlike the Bash-B seen in calcium imaging, where consecutive peaks occur before they can return to baseline. Therefore, the fact that $[Ca^{2+}]_i$ remains above baseline during the Bash-B episode is probably not due to persistent depolarization of membrane potential and resultant calcium entry, but to

Figure 5. Window current peaks at E12.5 and makes InZ cells more excitable
A–*C*, superimposed activation (open circle) and inactivation (filled square) current–voltage relations for voltage-gated inward current shown for E11.5 (*A*), E12.5 (*B*) and E13.5 (*C*). *D*–*F*, current–voltage relations for the averaged window current, extracted from the superimposed activation and inactivation curves in *A*–*C*. Mean resting membrane potential (V_{rest}), adapted from Watari *et al.* (2013), is indicated by arrows on the voltage axis. *G*, upper and lower voltage ranges of window current (grey) and voltage at which the window current peaks (black) at each stage. *H*, peak window current and peak inward current at each stage. *I*, current densities (in picoamperes per picofarad) for peak window and peak inward current at each stage. In *G*–*I*, E11.5, $n = 18$; E12.5, $n = 16$; and E13.5, $n = 7$. The error bars are SEM. *J*, a representative current-clamp trace recorded from a mid-line cell in r1 hindbrain during midbrain–hindbrain loops. *K*, waveform of a depolarizing event sampled from *J* (third event). *L*, a representative current-clamp trace recorded from a mid-line cell in midbrain tegmentum during midbrain–hindbrain loops. *M*, waveform of a depolarizing event sampled from *L* (third event). Scale bars represent 5 s (*J* and *L*) and 1 s (*K* and *M*).

an interval between membrane potential depolarizations shorter than the extrusion time, or clearance, of $[Ca^{2+}]_i$.

Midbrain cells are less excitable than hindbrain cells at E12.5

Similar to the hindbrain cells, current clamp of a mid-line cell in the midbrain tegmentum (150 μm rostral to the isthmus, within the looping circuit) shows each depolarizing event returning to the resting membrane potential during a midbrain–hindbrain loop (Fig. 5*L*). However, midbrain cells exhibit smaller peak amplitudes and longer plateaux than hindbrain mid-line cells (Fig. 5*M* compared with *K*). This suggests that the midbrain cells have different membrane properties from the hindbrain cells. To test this, we performed voltage clamp at three locations along the mid-line of the rostral brainstem, as shown in Fig. 6*A*, namely midbrain tegmentum 150 μm rostral to the isthmus (MB), hindbrain r1 (r1) and hindbrain r2 (r2). As the midbrain cells have a smaller membrane capacitance than the hindbrain cells (Fig. 6*C*), indicating smaller cell diameter, we calculated current densities per unit capacitance. The peak inward current and the peak window current were both smaller in midbrain cells than in hindbrain cells (Fig. 6*B*, *D* and *F*). The inward current density for midbrain cells (-6.0 ± 0.7 pA pF^{-1}, $n = 13$) is one-third of that for hindbrain cells (r1, -16.4 ± 1.2 pA pF^{-1}, $n = 10$; r2, -15.7 ± 2.0 pA pF^{-1}, $n = 16$; $P < 0.001$; Fig. 6*E*), suggesting that there are fewer voltage-gated ion channels that support depolarization in the midbrain. The outward current is similar in midbrain and hindbrain cells (Fig. 6*H*; MB, 353.7 ± 39.6 pA, $n = 13$; r1, 469.4 ± 44.5 pA, $n = 10$; r2, 334.5 ± 35.9 pA, $n = 16$; voltage stepped from –80 to +80 mV; $P = 0.063$), but when normalized to membrane capacitance, the resulting outward current density is significantly higher in the midbrain cells (Fig. 6*I*; MB, 34.7 ± 2.7 pA pF^{-1}, $n = 13$; r1, 22.7 ± 1.6 pA pF^{-1}, $n = 10$; r2, 18.4 ± 1.5 pA pF^{-1}, $n = 16$; MB *vs.* r1, $P < 0.01$; MB *vs.* r2, $P < 0.001$). Taken together, the midbrain cells have a higher density of voltage-gated ion channels that hyperpolarize rather than depolarize, which is consistent with the observation that spontaneous activity initiates in the hindbrain but not in the midbrain (Rockhill *et al.* 2009). Also, this lower excitability may explain the slower propagation of events in the midbrain tegmentum during Bash-B, which may contribute to the slower lap time in the loops that involve the midbrain.

Bash bursts cease by E13.5; can they be rescued?

Membrane properties of mid-line cells are similar between E12.5 and E13.5 (Fig. 5*B* and *C*, *E* and *F*, and *H* and *I*). This suggests that Bash-B could be supported at E13.5. However, Bash-B disappear by E13.5. One major difference between E12.5 and E13.5 is that outward current is larger at E13.5 (568.7 ± 76.1 pA at E13.5, $n = 7$ *vs.* 334.5 ± 35.9 pA at E12.5, $n = 16$; voltage was stepped from –80 to +80 mV; $P < 0.01$). The increased outward current could suppress subsequent events by repolarizing the membrane potential and by shortening the duration of each event (Spitzer, 2012), which may underlie the disappearance of Bash-B at E13.5. Acute bath application of 5 mM tetraethylammonium, which effectively reduces outward current to E12.5 levels (276.8 ± 39.5 pA, $n = 7$; $P < 0.01$ *vs.* control), increases event frequency but fails to induce Bash-B at E13.5 ($n = 3$, data not shown). This suggests that the absence of Bash-B is not due to increased outward current. To investigate alternative causes of the disappearance of Bash-B at E13.5, we attempted to evoke Bash-B by other means.

A number of neurotransmitter receptor agonists increase event frequency at E13.5 (Hunt *et al.* 2006*a*), including muscimol ($GABA_A$ agonist), AMPA (glutamate receptor agonist) and nicotine (nicotinic ACh receptor agonist). In particular, bath application of 100 μM nicotine initially increased the frequency of events that propagated along the mid-line and mimicked Bash-B ($n = 7$), even in the absence of an intact midbrain ($n = 3$). However, events did not propagate in loops, but instead were induced by a rapid firing of the InZ cells, or a group of cells that are more caudal than r2. Also, nicotine-induced Bash-B ended consistently after a few minutes. Thus, the mechanism underlying nicotine-induced high-frequency firing is probably different from the Bash-B that occur naturally at E12.5.

Another alternative is that the endogenous Bash-B may fail to occur at E13.5 because events can no longer loop, possibly due to a modification of the looping circuit. To visualize a possible change to the tracks, individual frames of video that showed propagation of events were combined into a single image at E12.5 (Fig. 7*A*) or E13.5 (Fig. 7*B*; see Methods). At E12.5, the resultant image revealed the tracks of event propagation spanning from the midbrain to r2 hindbrain (Fig. 7*A*). A line-intensity scan across the mid-line shows two peaks separated by 72.4 μm at the isthmus (isth), suggesting that calcium events propagate in two tracks. The two peaks in the line scan are also present in r1 hindbrain (200 μm caudal to the isthmus), where they are further apart (78.7 μm). The tracks are closer together (64.5 μm) at a position 400 μm caudal to the isthmus, and then converge as they get closer to r2, such that they cannot be discerned clearly (r2). The two peaks suggest that the rostral hindbrain has two separate tracks flanking the mid-line axis at E12.5 ($n = 4$). A line scan across the midbrain shows a single peak (MB, Fig. 7*A*), indicating that the parallel tracks along the mid-line axis of the hindbrain have converged in the midbrain tegmentum such that the events can cross to

the other side of the mid-line as a single track. Identical tracks are used by events that propagate in loops and those that are single events (data not shown), indicating that some events propagate in looping patterns whereas others do not.

In contrast to E12.5, the line scan analysis yields a single peak at the isthmus and r1 at E13.5 (Fig. 7*B*, $n = 4$). This suggests that E13.5 hindbrain uses a single track instead of two, which may reflect an alteration to the looping circuit itself, preventing propagation in loops. Furthermore, the calcium signal is fainter in the midbrain (Fig. 7*B*), indicating that the extent of propagation is limited in the midbrain tegmentum at E13.5. This may be caused by retraction, which is known to limit the spatial extent of event propagation in r5 hindbrain at E13.5 (Watari *et al.* 2013). To verify this, we compared passive membrane properties at different stages and positions (Fig. 7*C–H*). At E12.5, before retraction has occurred along the mid-line of the hindbrain (Watari *et al.* 2013), membrane resistance in the midbrain and r5 cells is similar (Fig. 7*D*). Resting membrane potential is also not different at these positions. This indicates that retraction has not yet occurred in the midbrain at E12.5. In contrast, at E13.5, membrane resistance is reduced in the midbrain to the same level as that in r5 (Fig. 7*G*), where we had previously demonstrated that the retraction process of hyperpolarization has already occurred (Watari *et al.* 2013). This makes the membrane less excitable, possibly hindering propagation of events into and across the midbrain tegmentum. Although midbrain cells do not hyperpolarize, unlike r5 cells (Fig. 7*H*), at both stages the resting membrane potential is outside the range of the window current (Fig. 7*E* and *H*). Taken together, spatial retraction in the midbrain and convergence of mid-line tracks in the hindbrain may cause a loss of the looping circuit, hence preventing Bash-B at E13.5.

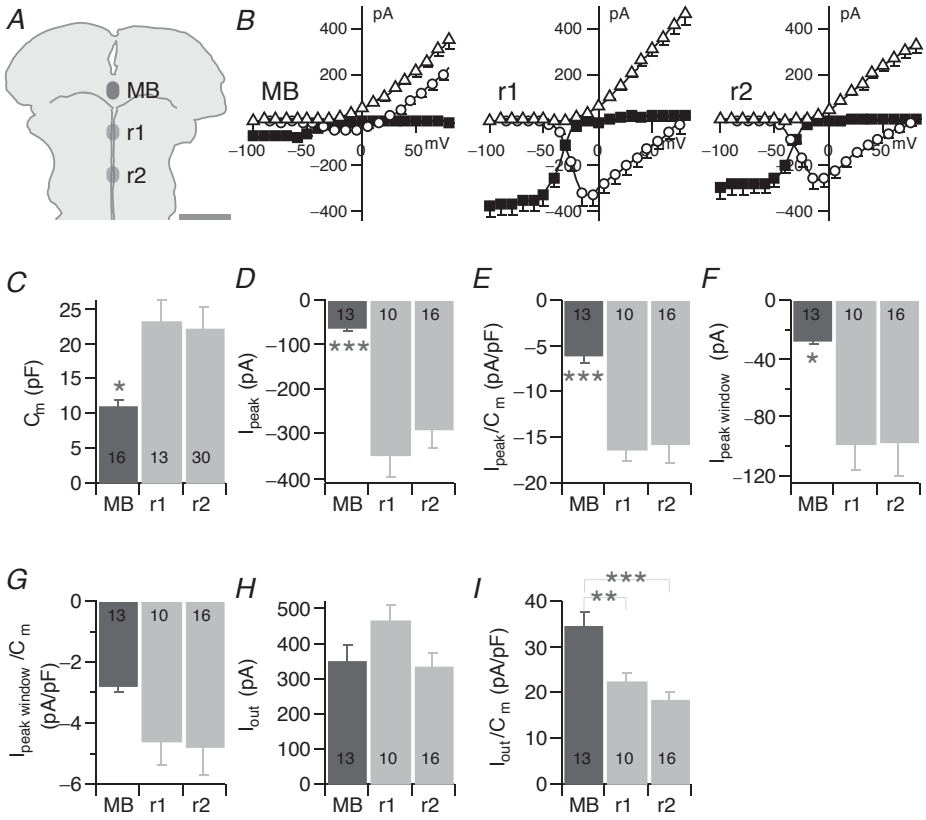

Figure 6. Midbrain cells are less excitable than hindbrain cells at E12.5, expressing less inward and more outward current densities
A, sites of patch-clamp recordings are as follows: midbrain tegmentum 150 μm rostral from isthmus and along mid-line axis (MB); r1 hindbrain 250–350 μm caudal from isthmus and 50 μm lateral to the mid-line axis, closer to one of the two parallel tracks (r1); and r2 hindbrain 50 μm rostral to cranial nerve V and along the mid-line axis, closer to one of the two parallel tracks (r2). Scale bar represents 1 mm. *B*, superimposed activation curve for voltage-dependent inward current (open circles), inactivation curve for voltage-dependent inward current (filled squares) and activation curve for voltage-dependent outward current (open triangles). *C*, membrane capacitance. *D*, peak inward current. *E*, peak inward current density. *F*, peak window current. *G*, peak window current density. *H*, peak outward current. *I*, peak outward current density. In *C–I*, $n \geq 10$ at each stage. The error bars are SEM.

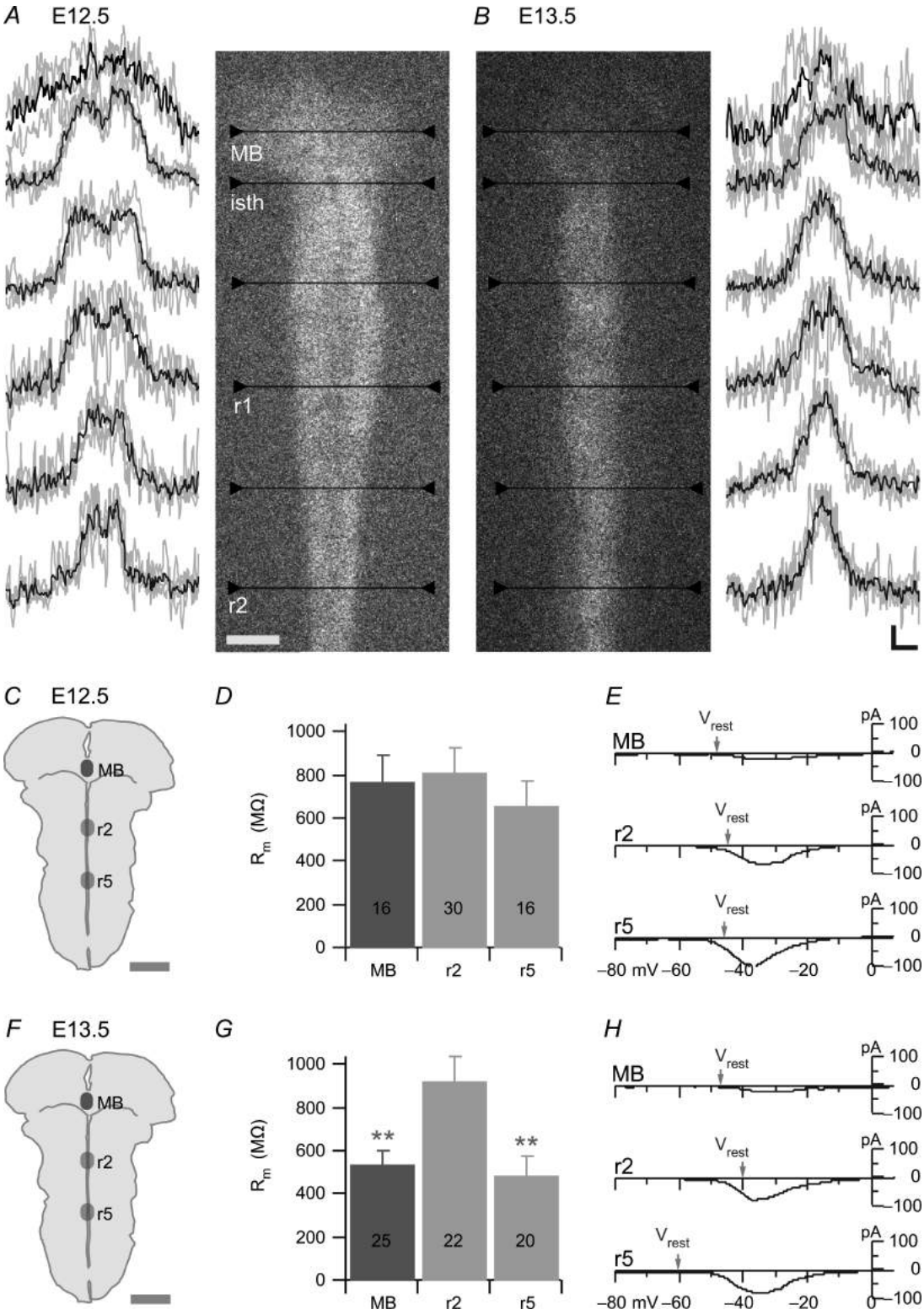

Why does looping not continue indefinitely?

We have observed the following four independent ways ($n = 18$ episodes in 15 experiments) in which the loops can end: via failures of propagation; a particular exit pattern in the midbrain; collisions of events; and branching into alternative tracks.

First, looping can end due to a propagation failure, which often occurs spontaneously in the midbrain tegmentum at or near the isthmus ($n = 7$ of 18; Fig. 8*A* and Movie 1).

The second way the loop can end involves a specific pattern of caudally directed exit from the midbrain tegmentum ($n = 6$ of 18; Fig. 8*B*). In some cases, events exit the midbrain back into the hindbrain along both mid-line tracks simultaneously. When this occurs, events propagate caudally down the hindbrain on both tracks and leave the looping circuit permanently.

Third, the looping event can collide with another event if they are travelling towards each other on the same track (Hughes *et al.* 2009) and this head-to-head collision causes both events to terminate ($n = 4$ of 18; Fig. 8*C*). The InZ cells, which fire independently of the looping event, initiate events that propagate rostrally (Fig. 8*C*, red arrows) and collide with the looping event (Fig. 8*C*, black arrow). Not every event from the InZ stops the looping event. A head-to-head collision typically occurs in the midbrain tegmentum, or in the hindbrain where events on two parallel tracks jump across the mid-line. The collision must be head to head, otherwise a component of an event may escape into an unoccupied track and continue to propagate along the looping circuit.

The fourth way to end Bash-B is sporadic branching of an event out of the looping circuit and into the lateral (dorsal) regions of the midbrain ($n = 1$ of 18; Fig. 8*D*), as described previously (Rockhill *et al.* 2009). This sudden branching pushes the event to propagate out of the looping circuit.

Taken together, an episode of Bash-B ends by a variety of methods and, as a result, the duration of Bash-B can vary widely from a few seconds (Fig. 1*C*, middle panel) to tens of minutes (Fig. 1*D*). The examples in Fig. 8*A*, *B* and *D* were taken from the same brainstem preparation, demonstrating that the brainstem is capable of ending loops by multiple means.

Discussion

A central dogma in neuroscience is that $[Ca^{2+}]_i$ is maintained at extremely low levels (30–200 nM) at rest (Hille, 2001). The duration of a typical action potential causing calcium entry is several milliseconds. This $[Ca^{2+}]_i$ is cleared within a few seconds, making the brief calcium signal a significant one, which influences processes including phosphorylation, apoptosis and gene expression. Here, we report a previously uncharacterized phenomenon, Bash-B, where $[Ca^{2+}]_i$ levels are sustained for an unusually long duration, in some cases longer than 10 min (Fig. 1*D*). This prolonged $[Ca^{2+}]_i$ increase may impact developmental processes such as proliferation, migration, axonal growth, synaptogenesis, ion channel expression and neurotransmitter specification (Moody & Bosma, 2005; Spitzer, 2012), by influencing gene expression in an activity-dependent manner (Flavell & Greenberg, 2008). Bash bursts emerge at E12.5 and disappear within 24 h, suggesting that they impact development in stage- and location-specific manners. The impacted neurons may include raphe serotonergic and ventral tegmental dopaminergic neurons, whose cell bodies and axons (Fig. 9*A* and *B*) are developing near or within the pathway of the events during Bash-B (Fig. 9*C*).

A looping circuit is a key underlying mechanism of Bash-B

Bash bursts are caused by a circuit where calcium events propagate in loops involving the mid-lines of the midbrain and hindbrain. Although each lap is brief (3–5 s), repetitive laps around this loop effectively extend calcium influx for minutes at a time. Each lap causes calcium influx at a rate faster than the clearance of calcium, resulting in

Figure 7. Calcium events do not loop at E13.5
A, right panel is a compiled image of the tracks spanning midbrain tegmentum and r2 hindbrain at E12.5. *A*, left traces are the results of the line intensity scans, normalized and superimposed (grey, $n = 4$) along with the averaged line (black). Scale bar represents 100 μm (for images in *A* and *B*). *B*, left panel is a compiled image of the tracks spanning midbrain tegmentum and r2 hindbrain at E13.5. *B*, right traces are results of the line intensity scans, normalized and superimposed (grey, $n = 4$) along with the averaged line (black). The positions of the line scans correspond to the lines with inverted arrowheads in the adjacent panel. Scale bar represents 0.2 normalized $\Delta F/F$, 50 μm (for line scan plots in *A* and *B*). *C*, positions of the patch-clamp recordings at E12.5 are as follows: midbrain tegmentum 150 μm rostral from isthmus and along mid-line axis (MB); r2 hindbrain 50 μm rostral to cranial nerve V and along mid-line axis, closer to one of the two parallel tracks (r2); and r5 hindbrain (r5). *D*, membrane resistance (MB, $n = 16$; r2, $n = 30$; and r5, $n = 16$). *E*, current–voltage relations showing averaged window current and location of average V_{rest} (arrows) at the three positions. *F*, positions of the patch-clamp recordings at E13.5. *G*, membrane resistance (MB, $n = 25$; r2, $n = 22$; and r5, $n = 20$). *E*, current–voltage relations showing averaged window current and location of average V_{rest} (arrows). The V_{rest} values are taken from Watari *et al.* (2013) for r2 and r5. The error bars are SEM. Scale bar represents 1 mm (*C* and *F*).

the characteristic above-baseline $[Ca^{2+}]_i$ of Bash-B. The looping mechanism allows cells to experience calcium influx at frequent and regular intervals, influencing processes that require sustained or pulsatile calcium input.

Window current may contribute to spontaneous activity but is not directly causative of loops

Each episode of Bash-B is triggered by an event initiated at the InZ, that then either propagates in loops (Fig. 4*A*–*D*) or, rarely, is followed by repeated firing from the InZ (without use of the looping circuit; Fig. 4*C*). In either case, the InZ is essential to triggering Bash-B. The repetitive firing is supported by decreased resting conductance, depolarized V_{rest} (Watari *et al.* 2013), increased voltage-gated inward current and increased window current (Fig. 5*H*). High membrane excitability in InZ cells at E12.5 is conducive to Bash-B and a probable cause of the non-looping, rapid-firing style of Bash-B (Fig. 4*C*). The inward current is predominantly T-type calcium current (Ca_V3) at E11.5 (Moruzzi *et al.* 2009); sodium current may contribute after this stage. Ca_V3 does not inactivate within a positive range of voltages, permitting persistent calcium influx called 'window current' that can be effective even at rest (Bean & McDonough, 1998). In developing spinal cord, the low threshold of T-type current activation plays a critical role in allowing spontaneous events when V_{rest} is substantially lower than the window of current (Gu & Spitzer, 1993). The window current based on T-type calcium current is postulated to regulate cell proliferation (Capiod, 2011). Coincidentally, the thickness of the brainstem from the ventricular zone to pial surface increases by 120 μm between E11.5 and E12.5 (Rockhill *et al.* 2009), indicating

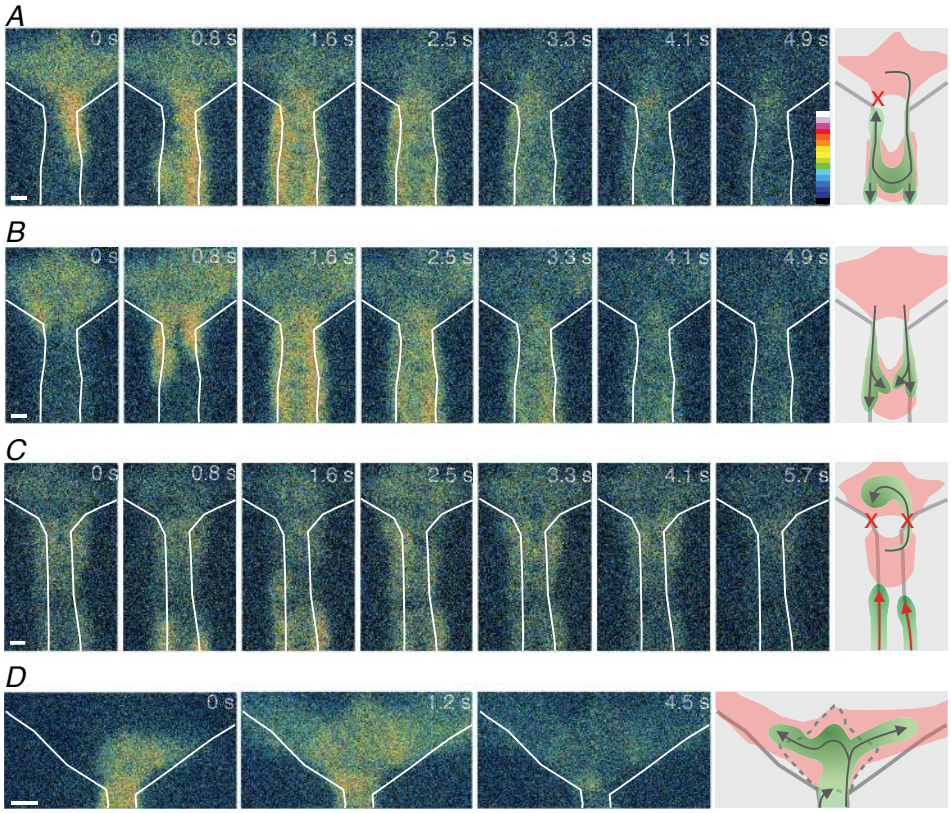

Figure 8. Four independent mechanisms that underlie the end of a looping pattern
A, an example of an event in the midbrain–hindbrain loop failing to propagate at or near the isthmus. X indicates the location of propagation failure. *B*, an example of an event exiting from both sides of the midbrain. *C*, an example of colliding wavefronts; an event in the midbrain–hindbrain loop (black arrow) collides at the isthmus with an event from the InZ (red arrow) on the left track. The event on the right track arrives at the isthmus slightly later than the left, and it fails to propagate into the midbrain, as described in *A*. X indicates the locations where propagation ends. *D*, an example of an event propagating dorsolaterally into the midbrain. The area of the midbrain tegmentum through which the event propagated during the loops is outlined with a dotted line. Examples in panels *A*, *B* and *D* were taken from the same brainstem preparation. The images are pseudocoloured to show relative intensity of $[Ca^{2+}]_i$ (white, high intensity; black, low intensity). Scale bars represent 50 μm (*A*, *B* and *C*) and 100 μm (*D*).

that cell proliferation correlates with the period when window current increases (Fig. 5*H*).

Given that V_{rest} is within the voltage range of the window current, this steady-state inward current may contribute to cell firing. In support of this, the mean V_{rest} is positioned within the voltage range of the window current at stages when spontaneous activity is robust (E11.5–13.5; Fig. 5*D*–*F*), whereas it hyperpolarizes below the range at later stages when spontaneous activity ceases (E14.5–15.5; data not shown) due to retraction (Watari *et al.* 2013). Therefore, the ability of a mid-line cell to support spontaneous activity, and the level of $[Ca^{2+}]_i$ increase, may depend on the V_{rest} relative to the voltage range of the window current. The ability of the cells to maintain elevated $[Ca^{2+}]_i$ levels is most probably due to a mismatch between the rates of calcium entry and clearance, as opposed to tonic calcium entry resulting from persistent depolarization.

Refractory period dictates the flow and directionality of calcium waves

The refractory period is proposed to regulate the spread of retinal waves (Butts *et al.* 1999), because the direction of wave propagation is dependent on the number of recruitable cells, which become refractory for some time after wave propagation. In the hindbrain, when two wave-fronts collide (head-to-head collision), propagation of both waves ends (Hughes *et al.* 2009). Waves cannot back-propagate, dictating a single direction of propagation for each event. Only where propagation is slower, possibly exceeding the refractory period, as in the mid-brain tegmentum, can events make U-turns and reverse direction. Therefore, a refractory period is likely to regulate both directionality and the termination of event propagation.

Variants of the looping circuit provide the means to vary the frequency of calcium input

The location of the looping circuit designates the interpeak interval of calcium events to either 3 s (hindbrain-only loops) or 5 s (midbrain–hindbrain loops). A combination of several properties of the midbrain may explain the slower lap time in midbrain–hindbrain loops, namely length of the path, delayed propagation at the isthmus and reduced membrane excitability. First, the path that encompasses the midbrain tegmentum is longer than that restricted to the hindbrain, lengthening single lap times. Second, propagating events appear to 'pause' as they reach the isthmus (Rockhill *et al.* 2009), and the resulting lag adds to the total lap time. Third, midbrain cells have a low density of inward current (Fig. 6*E*) and V_{rest} hyper-polarized to the voltage range of the window current (Fig. 7*E*); the resultant reduction in membrane excitability may contribute to slower propagation through the mid-brain. These factors, alone or in combination, may prolong the time it takes to complete a lap in midbrain–hindbrain loops. The underlying cells in a 5 s hindbrain-midbrain loop experience deeper valleys of $[Ca^{2+}]_i$ between events

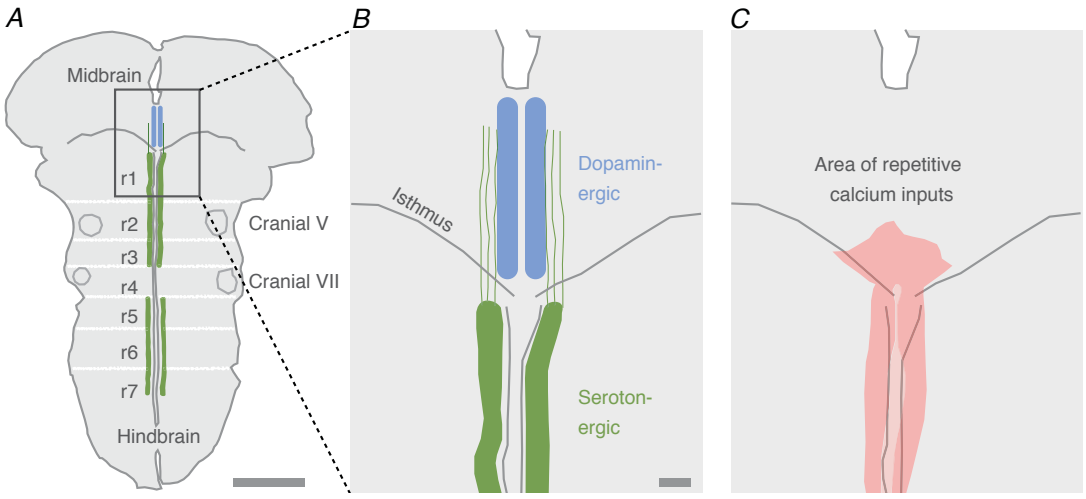

Figure 9. Possible effect of Bash-B on development
A, a mouse brainstem showing the location of the developing raphe serotonergic (hindbrain) and tegmental dopaminergic (midbrain) neurons at E12.5. For reference, white lines are drawn across the hindbrain to indicate the locations of the former rhombomeres (r1–r7). Scale bar represents 1 mm. *B*, a diagram of the mid-line isthmus shows the growth of serotonin axons, putative carriers of calcium events on the two parallel tracks flanking the mid-line (Rockhill *et al.* 2009), into the midbrain. Scale bar (applies to *B* and *C*) represents 100 μm. *C*, the same region as *B*, showing an area of repeated calcium inputs during Bash-B.

than 3 s hindbrain-only loops, which have a higher sustained $[Ca^{2+}]_i$. In developing spinal cord, $[Ca^{2+}]_i$ events of different shape and duration mediate different developmental functions (Gu *et al.* 1994). Our data would suggest that the brainstem can combine two looping circuits (Fig. 4*D*), each with a unique lap time, to fine-tune the total amount of calcium input.

Midbrain influences the fate of event propagation

A propagating event may enter or exit a looping circuit, change direction or fail altogether at the midbrain because of two 'barriers' regulating propagation in an all-or-none fashion. A probable mechanism of the barriers, one of which is found at the isthmus and the other between the midbrain tegmentum and dorsolateral regions of the midbrain, is incomplete chemical transmission. Across the latter border, propagation requires activation of a set of neurotransmitter receptors (ACh and GABA receptors; Rockhill *et al.* 2009), suggesting that crossing this border requires chemical transmission. The transmission may be immature or suboptimal in that propagation fails sporadically, ending the loops. The pause at the isthmus (Rockhill *et al.* 2009) may be inherent to incomplete track formation because the axon bundles of serotonergic neurons, putative carriers of calcium events on the two parallel tracks flanking the mid-line (Figs 7*A* and 9*B*), are still extending from the hindbrain into midbrain tegmentum (Rockhill *et al.* 2009). The calcium waves propagating across or near these borders during Bash-B may strengthen and fine-tune neurotransmission or specify receptor identities.

Neurotransmitter systems that support spontaneous activity change across stages

Variation of the calcium input during spontaneous activity homeostatically regulates specification of neurotransmitter phenotypes in the serotonergic system in the developing hindbrain of *Xenopus laevis* (Demarque & Spitzer, 2010; Spitzer, 2012). Changes in event frequency across stages in the mouse brainstem suggest that neurotransmitter systems could be a target for regulation by spontaneous activity. GABA, which is excitatory in many developing brain structures (Ben-Ari, 2002), increases event frequency at E13.5 but not earlier, at E11.5, in mouse hindbrain (Hunt *et al.* 2006*a*). Likewise, event frequency is modulated by noradrenaline at E13.5 but not at E11.5. AMPA and, to a lesser extent, NMDA increase event frequency more at E13.5 compared with E11.5 (Hunt *et al.* 2006*a*), and this trend progresses such that bath application of AMPA induces calcium events in quiescent hindbrain at later stages (Watari *et al.* 2013). In contrast, nicotine robustly increases event frequency at E13.5 (Hunt *et al.* 2006*a*) but has no effect at E15.5 (data not shown). Thus, transmitter systems change expression in the embryonic mouse brainstem. The sustained increases in $[Ca^{2+}]_i$ during Bash-B may influence this; more work is needed to study the impact of Bash-B in transmitter specification.

Bash bursts are a novel mechanism by which participating cells experience calcium influxes at frequent and regular intervals, leading to $[Ca^{2+}]_i$ above baseline levels for minutes, a markedly long time for an ion that typically is rigorously maintained at low cytoplasmic levels. This prolonged increase in $[Ca^{2+}]_i$ may influence cellular processes necessary to the development of participating and neighbouring cells, including raphe serotonergic and ventral tegmental dopaminergic neurons.

References

Bean BP & McDonough SI (1998). Two for T. *Neuron* **20**, 825–828.

Ben-Ari Y (2002). Excitatory actions of GABA during development: the nature of the nurture. *Nat Rev Neurosci* **3**, 728–739.

Bosma MM (2010). Timing and mechanism of a window of spontaneous activity in embryonic mouse hindbrain development. *Ann N Y Acad Sci* **1198**, 182–191.

Butts DA, Feller MB, Shatz CJ & Rokhsar DS (1999). Retinal waves are governed by collective network properties. *J Neurosci* **19**, 3580–3593.

Capiod T (2011). Cell proliferation, calcium influx and calcium channels. *Biochimie* **93**, 2075–2079.

Demarque M & Spitzer NC (2010). Activity-dependent expression of Lmx1b regulates specification of serotonergic neurons modulating swimming behavior. *Neuron* **67**, 321–334.

Flavell SW & Greenberg ME (2008). Signaling mechanisms linking neuronal activity to gene expression and plasticity of the nervous system. *Annu Rev Neurosci* **31**, 563–590.

Gu X, Olson EC & Spitzer NC (1994). Spontaneous neuronal calcium spikes and waves during early differentiation. *J Neurosci* **14**, 6325–6335.

Gu X & Spitzer NC (1993). Low-threshold Ca^{2+} current and its role in spontaneous elevations of intracellular Ca^{2+} in developing *Xenopus* neurons. *J Neurosci* **13**, 4936–4948.

Hille B (2001). *Ion Channels of Excitable Membranes*, 3rd edn. Sinauer Associates Inc.

Hughes SM, Easton CR & Bosma MM (2009). Properties and mechanisms of spontaneous activity in the embryonic chick hindbrain. *Dev Neurobiol* **69**, 477–490.

Hunt PN, Gust J, McCabe AK & Bosma MM (2006*a*). Primary role of the serotonergic midline system in synchronized spontaneous activity during development of the embryonic mouse hindbrain. *J Neurobiol* **66**, 1239–1252.

Hunt PN, McCabe AK, Gust J & Bosma MM (2006*b*). Spatial restriction of spontaneous activity towards the rostral primary initiating zone during development of the embryonic mouse hindbrain. *J Neurobiol* **66**, 1225–1238.

Momose-Sato Y, Nakamori T & Sato K (2012). Spontaneous depolarization wave in the mouse embryo: origin and large-scale propagation over the CNS identified with voltage-sensitive dye imaging. *Eur J Neurosci* **35**, 1230–1241.

Moody WJ & Bosma MM (2005). Ion channel development, spontaneous activity, and activity-dependent development in nerve and muscle cells. *Physiol Rev* **85**, 883–941.

Moruzzi AM, Abedini NC, Hansen MA, Olson JE & Bosma MM (2009). Differential expression of membrane conductances underlies spontaneous event initiation by rostral midline neurons in the embryonic mouse hindbrain. *J Physiol* **587**, 5081–5093.

Rockhill W, Kirkman JL & Bosma MM (2009). Spontaneous activity in the developing mouse midbrain driven by an external pacemaker. *Dev Neurobiol* **69**, 689–704.

Spitzer NC (2012). Activity-dependent neurotransmitter respecification. *Nat Rev Neurosci* **13**, 94–106.

Watari H, Tose AJ & Bosma MM (2013). Hyperpolarization of resting membrane potential causes retraction of spontaneous Ca_i^{2+} transients during mouse embryonic circuit development. *J Physiol* **591**, 973–983.

Additional Information

Competing interests

None declared.

Author contributions

Conception and design of the experiments, collection, analysis and interpretation of data: H.W. and A.J.T. Drafting the article or revising it critically for important intellectual content: H.W., A.J.T. and M.M.B. All authors have read and approved the final submission.

Funding

This work is supported by NSF IOS 0952395.

Acknowledgements

Special thanks to Bess Navarrete, Veronica Rodriguez, Ashley Lin, Curtis Easton and Joseph Bosma-Moody for technical assistance and to Bill Moody and Horacio de la Iglesia for critical reading of the manuscript. Thanks to Horacio de la Iglesia for lending us the ×4 objective lens that was crucial to this study.